UC Berkeley
UC Berkeley Previously Published Works

Title

Ultrafast dynamics in van der Waals heterostructures

Permalink

Journal

ISSN

Authors

Jin, Chenhao
Ma, Eric Yue
Karni, Ouri
et al.

Publication Date

DOI

Ultrafast dynamics in van der Waals heterostructures

Chenhao Jin[1], Eric Yue Ma[2], Ouri Karni[2], Emma C. Regan[1,3,4], Feng Wang[1,4,5]*, Tony F. Heinz[2,6]*

[1] Department of Physics, University of California at Berkeley, Berkeley, California 94720, USA.
[2] Department of Applied Physics, Stanford University, Stanford, California 94305, USA.
[3] Graduate Group in Applied Science and Technology, University of California at Berkeley, Berkeley, California 94720, USA
[4] Material Science Division, Lawrence Berkeley National Laboratory, Berkeley, California 94720, USA.
[5] Kavli Energy NanoSciences Institute at University of California Berkeley and Lawrence Berkeley National Laboratory, Berkeley, California 94720, USA.
[6] SLAC National Accelerator Laboratory, 2575 Sand Hill Road, Menlo Park, California 94025, USA.

* Correspondence to: tony.heinz@stanford.edu, fengwang76@berkeley.edu

Abstract

Van der Waals heterostructures are synthetic quantum materials composed of stacks of atomically thin two-dimensional (2D) layers. Because the electrons in the atomically thin 2D layers are exposed to layer-layer coupling, the properties of van der Waals heterostructures are defined not only by the constituent monolayers, but also by the interactions between the layers. Many fascinating electrical, optical, and magnetic properties have recently been reported in different types of van der Waals heterostructures. In this review we focus on unique excited-state dynamics in transition metal dichalcogenide (TMDC) heterostructures. TMDC monolayers are the most widely studied 2D semiconductors, featuring prominent exciton states and accessibility to the valley degree of freedom. Many TMDC heterostructures are characterized by a staggered band alignment. This band alignment has profound effects on the evolution of the excited states in heterostructures, including ultrafast charge transfer between the layers, the formation of interlayer excitons, and the existence of long-lived spin and valley polarization in resident carriers. Here we review recent experimental and theoretical efforts to elucidate electron dynamics in TMDC heterostructures, extending from time scales of femtoseconds to microseconds, and comment on the relevance of these effects for potential applications in optoelectronic and valleytronic/spintronic devices.

36 **Main text**
37 Advances in the isolation and manipulation of atomically-thin sheets of two-dimensional (2D) crystals,
38 starting with the investigations of graphene a decade ago, have ushered in a new era of basic
39 scientific research and technological innovation. 2D layers with diverse properties can now be
40 prepared separately and then stacked together to form new types of quantum materials, known as
41 van der Waals (vdW) heterostructures. The ability to combine materials with monolayer precision
42 enables the design and creation of functional 2D materials that do not exist in nature. Today we have
43 at our disposal a wide variety of atomically thin 2D layers, ranging from semiconducting MoS_2 and
44 insulating hexagonal boron-nitride (h-BN) to magnetic CrI_3 and superconducting $NbSe_2$, that can be
45 stacked one upon the other. Since the electrons in atomically thin layers are exposed, different
46 quantum states found in the individual layers can interact and couple to one another in ways that are
47 not possible in other systems.
48
49 VdW heterostructures constitute a vast family of new quantum materials, since they are defined not
50 only by the combination of constituent monolayer materials, but also by the stacking sequence and
51 relative crystallographic alignment of the layers. Further control of physical properties in 2D vdW
52 heterostructures can be achieved through the application of electrostatic gating and fields, as well as
53 substrate and strain engineering. Many fascinating physical phenomena have been reported in
54 different vdW heterostructures, as exemplified by transport measurements revealing Hofstadter
55 butterfly states, fractional Chern insulators, gate-tunable Mott insulators, unconventional
56 superconductivity, etc[1-7]. In addition to electrical transport, there has also been great progress in the
57 study of the optical properties and excited-state dynamics in vdW heterostructures. Here we review
58 the new dynamical phenomena that emerge in semiconducting vdW heterostructures composed of
59 stacked transition metal dichalcogenide (TMDC) layers. We focus our discussion on TMDC
60 heterostructures, since the individual TMDC layers, with their many distinctive and intriguing
61 properties, have already been well characterized and provide a strong basis for understanding the
62 emergent new properties of heterostructures.
63
64 TMDC semiconductors (MX_2 layers with 2H symmetry and M = Mo, W; X = S, Se, Te) exhibit direct
65 gaps at monolayer thickness. They feature strong light-matter interactions and dramatically enhanced
66 electron-electron interactions, with the optical properties largely defined by exciton states. The
67 exciton binding energies in monolayer TMDCs are hundreds of meV– as much as two orders of
68 magnitude larger than in typical bulk semiconductors like silicon or GaAs[8,9]. In addition, TMDC
69 monolayers provide a platform to investigate and control the valley degree of freedom — often
70 designated as valley pseudospin — associated with the energetically degenerate K and K' valleys and
71 accessible optically through the presence of valley circular dichroism. The valley pseudospin in TMDC
72 is, moreover, coupled to the electron/hole spin due to strong spin-orbit interactions[10,11].
73
74 Understanding the dynamic interplay and evolution of the charge, spin, and valley excitations in vdW
75 heterostructures is of fundamental scientific interest. It is also of central importance for many potential
76 applications of TMDC materials in optoelectronics, spintronics, and valleytronics. The dissociation of
77 optically excited excitons into free carriers is, for example, critical for photovoltaic devices, while the
78 ability to control and stabilize valley polarization is essential for valleytronic applications. The
79 formation of vdW heterostructures in TMDC layers can profoundly affect their excited-state dynamics,
80 ranging from the dissociation of intralayer excitons and the formation of interlayer excitons to the
81 relaxation of spin and valley polarization. The use of vdW heterostructures provides a powerful
82 platform to control and optimize the dynamic response of the constituent materials. In this review, we

83   survey recent progress in probing electron dynamics, extending from femtoseconds to microseconds,
84   in TMDC heterostructures. On short time scales (≲1ps), the dynamics is dominated by the charge
85   transfer and energy relaxation processes in the heterostructure. On longer time scales (≳1ps), the
86   recombination of interlayer excitons and relaxation of the spin and valley degrees of freedom become
87   relevant. The rate of these processes can vary by orders of magnitude depending on the configuration,
88   temperature, and doping of the heterostructure. We will also touch upon the dynamics of lateral
89   transport of spin and valley polarization in TMDC heterostructures. We describe the physical
90   mechanisms that underlie the different types of dynamic response in TMDC heterostructures and
91   distinguish the behavior from that of the constituent layers, as well as mention briefly the implications
92   for potential new technologies.

93

94   **Band alignment in TMDC heterostructures**
95   In describing the single-particle electronic states in a vertical TMDC heterostructure, most authors in
96   the literature consider the states to be largely localized within the individual layers. This approximation
97   holds well for electronic states close to the band gap due to unusually weak interlayer coupling in
98   TMDCs at the relevant K and K' points in the Brillouin zone (Fig. 1a)[12]. Therefore one can directly
99   examine the relative energy difference, or band alignment, of material-specific electronic band
100 extrema, just as is commonly done for heterostructures and quantum wells based on bulk
101 materials[13,14]. An important distinction for atomically thin layers is that the concept of band bending
102 near an interface does not apply[15].

103

104 Semiconductor heterostructures can have different types of band alignment depending on the energy
105 difference of the conduction and valence band extrema in the constituent layers (Fig. 1b) [13,14]: The
106 lowest-lying states for electrons and holes reside in the same layer for a type-I heterostructure[16], but
107 are separated in different layers for a type-II heterostructure[13,17]. Further offsets in energy could, in
108 principle, lower the conduction band minimum (CBM) of one layer to a position below the valence
109 band maximum (VBM) of the other layer, yielding a type-III heterostructure[18].

110

111 The type of band alignment has profound effects on the excited-state dynamics in a vdW
112 heterostructure. In a type-I heterostructure carriers can only flow from the layer with the larger band
113 gap to the layer with the smaller band gap (assuming that they do not have excess energy greater
114 than the band offsets). The same applies to energy transfer through the exchange of virtual photons.
115 In a type-II heterostructure, on the other hand, electrons accumulate in the layer with the lower CBM,
116 while holes accumulate in the other layer[17,19,20]. Energy transfer can, however, still occur from the
117 larger-gap to the smaller-gap material[21].

118

119 There have been numerous theoretical studies of the band alignment in TMDC
120 heterostructures[13,14,18,22-24]. The result of one recent calculation is shown in Fig. 1c. Many of the
121 theoretical studies make use of DFT or related methods and cannot accurately account for the effects
122 of doping (Fermi level difference), dielectric screening, and excitonic interactions[25]. They provide
123 nonetheless guidelines for realizing specific types of heterostructures and combination of band gaps.
124 Although theoretical studies are advancing rapidly, at present a definitive determination of
125 heterostructure band alignment must rely on experiment[26,27].

126

127 In the following, we describe experimental findings concerning the dynamics of charge and energy
128 transfer for representative TMDC heterostructures, followed by a summary of the relevant theoretical
129 studies.
130
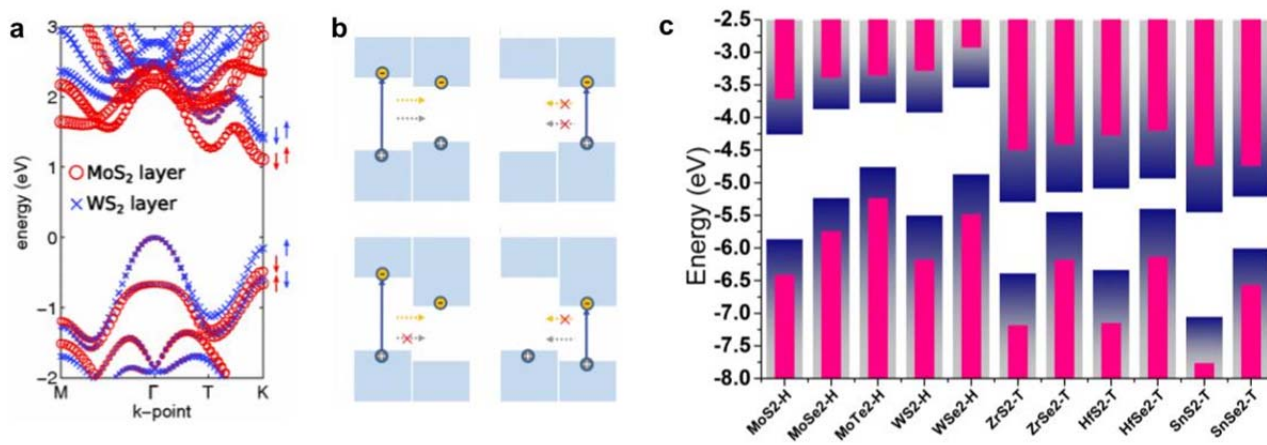
131
132 **Fig. 1 Band alignment in vertical vdW heterostructures of TMDCs**. (a)
133 Calculated electronic states in a MoS_2/WS_2 vertical heterostructure,
134 showing layer-localized states near the band edges at the K point[12]. (b)
135 Schematic of allowed charge transfer in heterostructures with type-I (top)
136 and type-II (bottom) band alignment[16]. (c) Calculated band-edge energies
137 for various TMDCs[22] based on different theoretical treatments: DFT-PBE
138 (blue) and G_0W_0 (pink).

139 **Charge transfer and energy transfer in TMDC heterostructures - Experiment**

140 Following the predictions of type-II band alignment in TMDC heterostructures, several experimental
141 studies were reported that aimed (among other goals) to validate these theoretical results by probing
142 the associated charge transfer (CT) or energy transfer (ET) processes. Vertical heterostructures have
143 been examined for various material combinations prepared with different fabrication methods,
144 including stacking of layers exfoliated from bulk crystals and from layers grown by chemical vapor
145 deposition (CVD), as well as heterostructures grown directly by CVD.
146
147 Ultrafast optical measurements using pump-probe spectroscopy provide the possibility of accessing
148 charge and energy transfer processes with femtosecond (fs) time resolution. In initial experiments,
149 Hong *et al*. examined the dynamics of the MoS_2/WS_2 heterostructure. Following excitation by an
150 ultrafast laser pulse resonant with the lower-energy MoS_2 A exciton, they observed a transient change
151 in reflectivity near the *higher-energy* WS_2 exciton (Fig. 2a)[19]. Based on theoretical predictions of type-
152 II band alignment of the two materials, this transient response was identified as arising from CT of a
153 hole from the MoS_2 monolayer to the WS_2 monolayer. By deconvolving the instrument response from
154 the rise-time of the signal, the authors were able to provide an upper limit of 50 fs for the charge
155 transfer time. Ceballos *et al.* observed similar dynamics in a heterostructure of MoS_2/$MoSe_2$, without
156 spectrally resolving the reflection of the probe[28]. They concluded, based on the theoretically predicted
157 band alignment, that electrons were transferred from $MoSe_2$ to MoS_2. In addition, when exciting both
158 layers (using excitation resonant with the higher-energy exciton feature in MoS_2) and comparing the

159 transient reflectivity signal of the monolayers to that of the heterostructure, the authors identified the
160 presence of hole transfer in the opposite direction, *i.e.*, from MoS_2 to $MoSe_2$ (Fig. 2b).
161
162 Following these first experimental investigations, several groups examined the nature of the ultrafast
163 CT for different types of heterostructures under different conditions. Heo *et al.* compared CVD-grown
164 and manually stacked WS_2/MoS_2 heterostructures with a focus on the dependence on the relative
165 (twist) angle of the two constituent lattices[29]. Measuring the transient transmission of the probe signal,
166 they did not resolve differences in the rise time of the signal associated with CT, but did observe a
167 pronounced difference in the decay times of the signal. Wang *et al.* examined several WSe_2/WS_2
168 heterostructures composed of CVD-grown layers mechanically stacked with different twist angles[20,29].
169 Using pump-probe measurements, together with steady-state techniques such as reflection contrast
170 spectroscopy, they showed the same ultrafast signature from the onset of CT, either from electrons
171 moving from WSe_2 to WS_2 or from holes traveling in the opposite direction. They concluded that
172 interlayer CT takes place within 450 fs, close to the duration of the pump pulses in their experiment,
173 and does not exhibit measurable sensitivity to the twist angle. Further reinforcing this conclusion, Zhu
174 *et al.* explored deterministically aligned heterostructures of mechanically exfoliated MoS_2 and WSe_2;
175 they that the CT signal appears within 40 fs regardless of twist angle (Fig. 2c)[30]. On the other hand,
176 the time scale of the decay was varied with the twist angle, but without any clear trend. Ji *et al.*
177 reported a similar CT rise time for stacks of CVD-grown MoS_2 and WS_2 (Ref [31]). Such rapid interlayer
178 CT irrespective of crystal orientation (and thus crystal momentum) is somewhat unintuitive. Chen *et*
179 *al.* probed intraband transitions in a heterostructure using infrared light and suggested a potential
180 explanation based on the rapid formation of "hot" interlayer excitons[32]. Additional theoretical
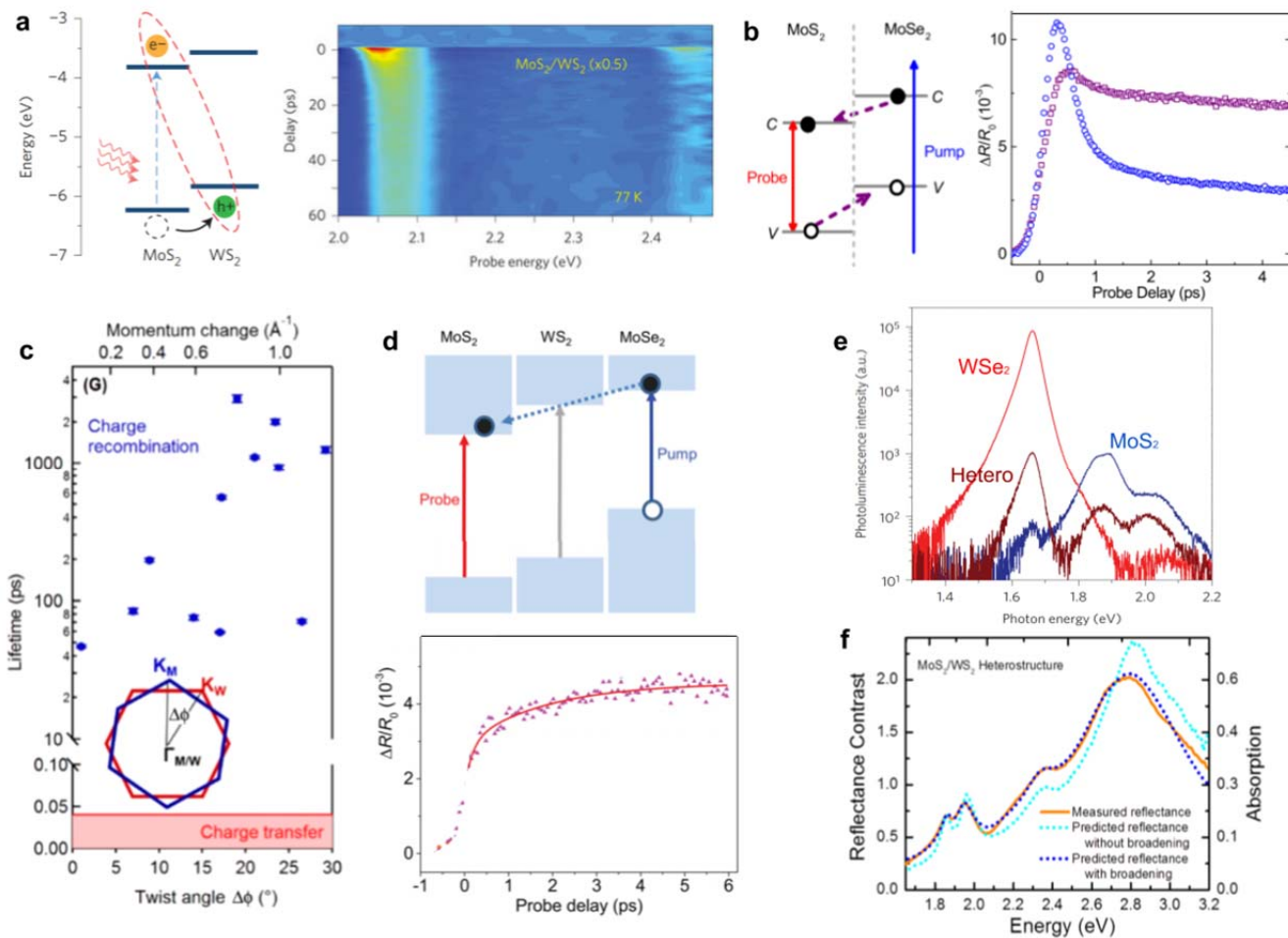181 investigations are summarized in the next section.
182

Fig. 2 Experimental studies of ultrafast charge transfer in vertical TMDC heterostructures. (a) Schematic and energy-resolved transient absorption spectra of a MoS_2/WS_2 heterostructure, excited by an optical pulse near the lower-energy MoS_2 A exciton feature, indicating hole transfer[19]. (b) Schematic and time-resolved differential reflection of a $MoS_2/MoSe_2$ heterostructure (blue) and of monolayer MoS_2 (purple), excited by an optical pulse above the band gaps of both materials, indicating both electron and hole transfer[28]. (c) Charge transfer (red shading) and recombination (blue) times in heterostructures of MoS_2 and WSe_2 with different twist angles, as indicated[30]. (d) Differential reflection at the energy of the MoS_2 A exciton following excitation at the energy of the $MoSe_2$ A exciton in a $MoSe_2/WS_2/MoS_2$ trilayer heterostructure[33]. (e) PL quenching[34] in MoS_2/WSe_2 and (f) broadening of the features absorption features[35] in a MoS_2/WS_2 heterostructure compared to the response of the separated monolayers.

Further demonstrating its robustness, the signature of ~ps electron transfer was observed in a trilayer heterostructure where monolayers of $MoSe_2$ and MoS_2 were separated by a monolayer WS_2 (Fig. 2d, Ref [33]). The authors suggested that such rapid CT across multiple materials is coherent, rather than sequential.

205 CT dynamics was also revealed in investigations of the coupling between pairs of TMDC layers. CT in
206 a MoS$_2$/MoTe$_2$ heterostructure was identified using pump-probe experiments[36], leading to the
207 suggestion of MoTe$_2$ as a good electrical contact for other semiconducting TMDCs and metals. Later,
208 cascaded transfer of electrons and holes across several TMDCs heterostructures was invoked to
209 explain correlated blinking observed in the photoluminescence (PL) in those stacks[37].

211 In addition to these time-resolved pump-probe measurements, CT between two TMDC layers in a
212 heterostructure has been inferred from quenching of the photoluminescence of the constituent
213 monolayers[19,20,28-33,38-40] and by broadening of the resonant features in the monolayers in optical
214 absorption measurements[20,35], both phenomena arising as a consequence of the presence of
215 additional relaxation channels in the heterostructures. A reduction in the PL intensity by factor of a few
216 tens to a few hundreds has commonly been observed (Fig. 2e)[19,34]. This suggests a corresponding
217 ratio for the charge transfer time compared to the population lifetime in the isolated material.
218 Assuming the latter to be a few hundred picoseconds for excitons in monolayer TMDCs[41] at room
219 temperature, we estimate a CT time of ~1 ps, somewhat longer than measured by pump-probe
220 techniques. This discrepancy can be explained as the result of a small fraction of the heterostructure
221 exhibiting poor contact between the layers, thus yielding reduced PL quenching compared to that of
222 the ideal structure. In optical absorption measurements, linewidth broadening of heterostructures
223 compared with that of the separate monolayers has been reported and used to estimate non-radiative
224 decay rates comparable to those deduced from pump-probe experiments (Fig. 2f)[35]. Extrinsic factors,
225 such as strain introduced in fabricating the heterostructure, can potentially also play a role. The
226 extremely rapid (few femtosecond) relaxation times inferred for high-lying states may, however,
227 remain difficult to probe directly in the time domain, but is easily observable by lineshape analysis.

229 Another dynamic process that may compete with CT is energy transfer (ET). In this latter process, an
230 exciton created in one layer recombines, and the released energy creates an exciton in the other layer.
231 Kozawa *et al.* reported evidence for such a process in a MoSe$_2$/WS$_2$ heterostructure (Ref [21]) on the
232 basis of a measured enhancement of PL from the MoSe$_2$ feature under excitation resonant with the
233 WS$_2$ optical band gap. Recently, ET was also identified in heterostructures of MoS$_2$ and WS$_2$
234 separated by insulating layers of h-BN[42]. In these structures, PL quenching from the heterostructure
235 was reduced, or even become PL enhancement, upon increasing the thickness of the h-BN spacer.
236 This was interpreted as an ET process between B excitons in MoS$_2$ and A excitons in WS$_2$. The
237 dependence of the enhancement on spacer thickness, with an optimum of PL enhancement for ~5
238 layers of h-BN and subsequent reduction of this effect with increasing layer thickness, is compatible
239 with the predicted trend for a dipole-dipole interaction. This highlights the major difference between
240 ET and CT processes: While the latter requires intimate coupling of the two constituent monolayers,
241 the former, originating in dipole-dipole interactions, can act at greater distances and across insulating
242 spacers. Although this difference between the processes is clear, there is currently little direct
243 experimental information on the absolute rates of energy transfer for TMDC layers and in what
244 regimes and under what conditions energy transfer competes with charge transfer.

245 **Charge transfer and energy transfer in TMDC heterostructures – Interpretation and theory**

246 Since most experiments have excited and probed excitonic resonances of the constituent layers, it
247 has often been assumed that CT occurs between their direct band-edge (K/K' valley) states. Band
248 structure calculations have shown that the K/K' states are localized around the central layer of metal
249 atoms and have weak interlayer interactions. On the other hand, for states of different momentum,

250   such as in the Γ or Q valleys, the interlayer coupling may be significantly stronger. One consequence
251   of this difference is the transition from indirect to direct band gap upon thinning TMDCs to the
252   monolayer limit: the bulk CBM in the Q valley, more affected by interlayer coupling, lies above the K
253   valley in monolayers[43,44]. For the same reason, the K-valley states are not expected to show such
254   rapid interlayer charge transfer. This contradiction with experiment is further heightened by the
255   apparent independence of CT on twist angle and lattice mismatch, the factors that dictate the
256   momentum difference between the initial and final states, as well as its insensitivity to temperature.
257   Here we briefly survey some of the approaches presented in the literature to identify the mechanism
258   responsible for the very efficient CT processes observed experimentally in vertical TMDC
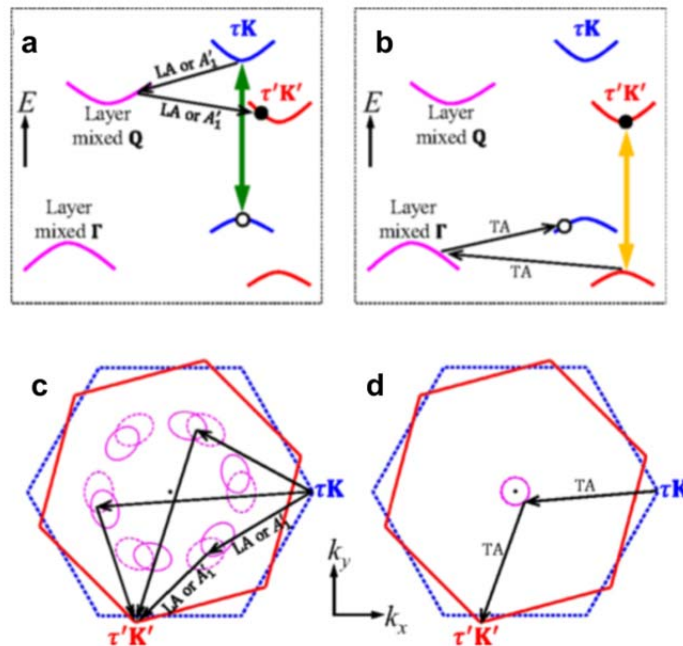259   heterostructures.
260
261   Zhu et al., following considerations relevant for CT processes in molecular systems, have pointed out
262   the possible role of localization in bridging the momentum mismatch[45]. The electrostatic attraction
263   between the optically excited electron and hole, which leads to the formation of tightly bound excitons,
264   gives rise to a distribution of momenta for the charge carriers across a significant range wavevectors
265   in the Brillouin zone (BZ). This situation could explain the apparent lack of momentum conservation in
266   the observed CT process. However, it is unclear with this effect alone could supply the large
267   momentum required for CT in heterostructures with large twist angles[30]. In addition, for excitation
268   substantially above the band gap, it is unclear whether exciton formation occurs prior to charge
269   transfer[28].
270
271   Several groups have also employed numerical calculations using molecular dynamics (MD) and time-
272   dependent density-functional theory (TD-DFT) to elucidate the mechanism for interlayer charge
273   transfer. Since accurately accounting for the effect of excitons is computationally demanding, these
274   calculations have focused on the transfer of free charge carriers from one monolayer to its neighbor.
275   Wang et al. described a process of transferring holes directly between the K valleys of the two layers
276   mediated by the electric dipole interaction of the initial and final states, which enhances the coupling
277   between the states to above a critical level for collective charge transfer[46]. In this description, both
278   twist angle and temperature have a significant influence on the transfer rate[46]. Zhang et al. pointed
279   out the significance of such dipole coupling between specific states in the vicinity of the K valley and
280   highlighted the expected twist-angle dependence of the CT rate[47]. Additionally, the authors argue that
281   the omission of excitonic effects for above gap excitation may not be significant if the time scales for
282   CT and exciton formation are comparable. (This argument is, however, problematic for explaining CT
283   from excitons created directly by resonant excitation.)
284
285   A slightly different picture is presented by Long et al.[48] and by Li et al.[49] for CT processes in
286   MoSe$_2$/MoS$_2$ and MoS$_2$/WS$_2$ systems, respectively. They propose that holes and/or electrons undergo
287   transfer from one layer to the other due to mixing between the electronic states near the K point of
288   both layers[48,49]: the states into which the charge carriers are optically injected are coherently mixed
289   (and therefore delocalized) across the two layers, so that CT need only to be driven by an intralayer
290   relaxation process to the K-valley, mediated by phonon emission. In this model, the coupling relies on
291   specific layer orientations to facilitate the state mixing in the heterostructure. The discrepancy
292   between this requirement and the apparent twist-angle independence of CT in experiments is
293   explained in terms of changes in the relative local atomic positions in the two layers across the moiré
294   pattern of the heterostructure[50,51]. Regardless of the twist angle of the layers, such lateral
295   inhomogeneity provides regions where the coupling between the layers is strong[31]. In all of the above
296   scenarios, phonons are necessary for the completion of the CT process, but not for its initiation.

297

298 Recent work has also explored a more direct role for phonons in the initiation of CT. Wang *et al.*

299 considered momentum-conserving charge transfer between the layers in various regions of the BZ,

300 including at the K, Q and Γ points for different twist angles and degrees of lattice mismatch[52], as

301 shown in Fig. 3a-d. The proposed mechanism involves scattering by phonons from the K valley to the

302 Γ valley (for holes) or to the Q valley (for electrons), regions where the interlayer coupling is strong

303 and interlayer charge transfer is rapid. After charge transfer, scattering with another phonon would

304 bring the charge carriers back to the K-valley. For intralayer scattering within 20 fs, the entire charge

305 transfer process would occur in less than 100 fs, as observed experimentally. A similar scheme was

306 developed by Zheng *et al.* using a numerical MD TD-DFT calculation, although without accounting for

307 inhomogeneities from the moiré pattern[53]. These theories better match the observed twist-angle

308 independence, as the coupling around the Γ and Q points is not sensitive to the layer orientation. The

309 expected temperature dependence of this mechanism is also weak, as it only requires emission of

310 phonons to dissipate the excess energy available from the transfer. This general mechanism has

311 been adopted in the interpretation of recent experiments related to CT processes[30,33,39].

312

313
314

315 **Fig. 3 Theoretical concepts explaining the robust and ultrafast**

316 **nature of CT in TMDC heterostructures**[52]**.** (a) Schematic representation

317 of phonon mediated electron transfer. (b) The same for hole transfer. (c)

318 Top view of the twisted BZ of the two layers, where electron transfer

319 between the K-points is mediated by phonon coupling to the Q-point. (d)

320 The same for hole transfer, mediated in this case by the coupling to the

321 Γ-point.

322

323

Spin and valley dynamics in TMDC heterostructures

The previous sections addressed carrier dynamics in TMDC heterostructures on the ultrafast time scale ($\lesssim$1ps) relevant for interlayer charge transfer in systems with type-II band alignment. In the following section, we focus on spin and valley relaxation dynamics in TMDC heterostructures, which take place on considerably longer time scales.

Within a TMDC monolayer, there are two distinct relaxation processes to consider. First, the population decay of optically excited excitons has a characteristic time scale of few picoseconds to nanoseconds, depending on choice of material, sample preparation, temperature, etc.[54-58]. Second, the exciton spin-valley lifetime, which determines how long information can be stored in the spin-valley degree of freedom, has been found to be a few picoseconds in isolated monolayer TMDCs[59-63]. Both the population and the spin-valley lifetimes in type-II heterostructures, where the electrons and holes reside in different layers after the rapid initial charge transfer process, can differ markedly from the corresponding lifetimes in isolated monolayers.

Below we review recent experimental results on dynamics on the pico-to-micro-second time scale in heterostructures and show that both the population lifetime and the spin-valley lifetime can be significantly longer than for the monolayer case. We then summarize recent efforts towards understanding the physical mechanisms of the corresponding intervalley scattering processes. Finally, we discuss the spatio-temporal dynamics of spin and valley polarization in TMDC heterostructures.

Long spin and valley lifetime in TMDC heterostructures

Traditional electronic devices are based on the manipulation of electron charges in the real space. Using other electron degrees of freedom as the information carrier, such as spin and valley, can potentially overcome fundamental limits of speed and power consumption, giving rise to intriguing new concepts in spintronics and valleytronics. A long spin/valley lifetime is necessary to ensure that the spin/valley information will be maintained in the idle state and can persist long enough to be processed. We note that the valley lifetime discussed here should not be confused with the valley depolarization time: the former can originate from different mechanisms, including the population decay of the valley information carriers, while the latter only describes the intervalley scattering process.

TMDCs offer a promising platform for spintronic and valleytronic applications, owing to several attractive properties of these materials. The valley-dependent optical selection rule allows for convenient creation, manipulation, and detection of excitons in specific valleys with circularly polarized light[64-66]. Furthermore, the spin-valley locking effect suggests that a very long spin-valley lifetime is possible because intervalley scattering of electrons or holes requires both a large momentum change from K to K' and a simultaneous spin flip[10,11]. However, several groups have measured exciton spin-valley dynamics using time-resolved Kerr rotation (TRKR)[59-63], and the spin-valley lifetime was found to be rather short, ranging from one to few picoseconds, even at low temperatures. This counter-intuitive observation was later explained as a consequence of the exchange interaction between excitons in the two valleys[67-70]: a bright exciton always has total momentum and spin of zero and therefore does not require any change in momentum or spin to scatter to the other valley as an intact exciton. This reduced spin-valley lifetime of excitons in TMDC monolayers significantly limits their use in carrying spin-valley information.

369

370 A general strategy for improving the spin-valley lifetime in TMDCs is to eliminate the exciton exchange
371 interaction by converting excitons into other excitations that serve as alternative carriers of valley
372 information. An additional figure of merit, the conversion efficiency, must be introduced to quantify the
373 final valley imbalance created from each optically excited exciton. To avoid loss of valley information
374 during conversion, the time scale of the conversion process (*i.e.*, the exciton population lifetime) must
375 be comparable to or shorter than the picosecond spin-valley lifetime of excitons. In monolayer TMDCs,
376 several candidates have been considered as the alternative information carriers, including trions[71-73],
377 dark excitons[74,75], biexcitons[76,77], and resident carriers[78-81]. For example, Fig. 4a,b show the valley
378 dynamics of trions and resident electrons probed by TRKR measurement. Unlike bright excitons,
379 these excitations have non-zero total momentum and/or total spin, and therefore will not suffer from
380 rapid spin-valley relaxation through the exchange interaction. Their spin-valley lifetimes at low
381 temperatures range from tens of picoseconds to a microseconds, but the conversion efficiency from
382 the initially generated exciton has rarely been characterized. However, since the exciton population
383 lifetime is comparable to or longer than the exciton spin-valley lifetime in these cases, the valley
384 conversion efficiency is likely to be considerably less than unity.

385

386 On the other hand, the interlayer charge transfer process in type-II heterostructures provides an
387 attractive mechanism to break intralayer excitons on the femtosecond time scale. As discussed above,
388 the ultrafast charge transfer process occurs very rapidly, typically within ~50 fs, in TMDC
389 heterostructures[19,82]. Because this time scale is much faster than exciton spin-valley relaxation, the
390 loss of spin-valley information during the conversion process is expected to be minor.

391

392 In nearly aligned heterobilayers, electrons and holes can form bright interlayer excitons after the
393 charge transfer process[28,40,83]. Rivera *et al*. observed 40% positive circular helicity from interlayer
394 exciton emission in WSe_2/$MoSe_2$ bilayer and measured a spin-valley lifetime of a few nanoseconds in
395 a time-resolved photoluminescence (TR-PL) study[84], as shown in Fig. 4c. The significantly longer
396 spin-valley lifetime of interlayer excitons can be understood by noting that the electron and hole
397 wavefunctions have much smaller overlap in interlayer excitons compared to intralayer excitons; they
398 will therefore have a weaker exchange interaction and exhibit slower recombination processes (both
399 radiative and non-radiative).

400

401 Recently, there has been increasing research interest in the nature of the interlayer exciton state and
402 the origin of the circular helicity of emission in nearly aligned heterostructures. Hsu *et al*. reported
403 negative circular helicity of interlayer exciton emission[85] in WSe_2/$MoSe_2$ bilayer, while Ciarrocchi *et al*.
404 and Hanbicki *et al*. observed two separate interlayer exciton emission peaks with opposite signs of
405 helicity[86,87]. Meanwhile, various configurations of interlayer excitons have been proposed as the
406 emitting state, including spin singlet zero-momentum excitons[84,88], spin-triplet zero-momentum
407 excitons[89], and finite-momentum excitons[90,91]. The rich set of observations originates in part from the
408 complex conduction band structure in the WSe_2/$MoSe_2$ bilayer, where electron states of spin up and
409 spin down, and at K and Q valleys, are all close in energy. Furthermore, the real-space distribution of
410 interlayer excitons when a moiré pattern is present can further modify the optical selection rules [92,93].
411 The exact mechanisms behind these interesting observations are yet to be fully understood.

412

413 An alternative approach involves using single-particle states, such as holes in WSe_2 to carry valley
414 information in the heterostructure. Because the momentum match between electrons and holes
415 (required for efficient exciton emission) is not relevant in this approach, a large-twist-angle bilayer is

416 preferred to separate electrons and holes in momentum space and further reduce their exchange
417 interaction and recombination rate. Kim *et al.* measured the spin-valley lifetime of holes in
418 WSe_2/MoS_2 heterostructures using circularly polarized pump-probe spectroscopy[94]. Figure 4d shows
419 the measured decay dynamics of the total hole population and valley-polarized hole population in the
420 WSe_2 layer at a temperature of 10 K. Both the population lifetime and the spin-valley lifetime of holes
421 are around one microsecond, indicating that the decay of the spin-valley imbalance occurs primarily
422 through population loss. On the other hand, the valley polarization remains almost a constant for a
423 few microseconds, from which one can extract a valley depolarization time (or intervalley scattering
424 time) exceeding 40 μs. The other critical figure of merit, the conversion efficiency, was also
425 determined experimentally to be close to unity for valley-polarized holes[94]. The nearly ideal
426 conversion efficiency is consistent with an interlayer charge transfer process that is far faster than
427 intervalley scattering processes.
428
429 The spin-valley lifetime of resident holes in the heterostructure can be further improved by tuning the
430 carrier concentration. Figure 4e summarizes the doping-dependent spin-valley lifetime of holes in a
431 WSe_2/WS_2 heterostructure (red circles), as compared to the population lifetime of holes (blue
432 triangles)[95]. In charge neutral and electron-doped heterostructures, the spin-valley lifetime is similar to
433 the population lifetime; however, for hole-doping, the spin-valley lifetime becomes orders of
434 magnitude longer than the population lifetime. This doping dependence is a consequence of the
435 interlayer electron-hole recombination process, as shown in Fig. 4f,g. For electron-doped or charge
436 neutral heterostructures (Fig. 4f), all of the holes in WSe_2 are pump-generated excess holes.
437 Therefore, when hole population decays to zero due to interlayer electron-hole recombination, no
438 holes -- and certainly no valley-polarized holes -- remain in the WSe_2. The valley lifetime is then
439 limited by the lifetime of the total hole excess. On the other hand, if the original hole density is much
440 greater than the photo-generated density, excess electrons in WS_2 will recombine with holes from
441 both valleys of WSe_2 with nearly equal probability (Fig. 4g). Consequently, a pure spin-valley
442 imbalance (*i.e.*, equal excess and deficiency of holes in the K and K' valley) is generated, the lifetime
443 of which can be much longer than the population lifetime and has been found to exceed 20 μs.
444 Furthermore, the decrease of spin-valley imbalance is negligible during the population decay, and the
445 overall efficiency of this two-step conversion process can approach 100%[95].
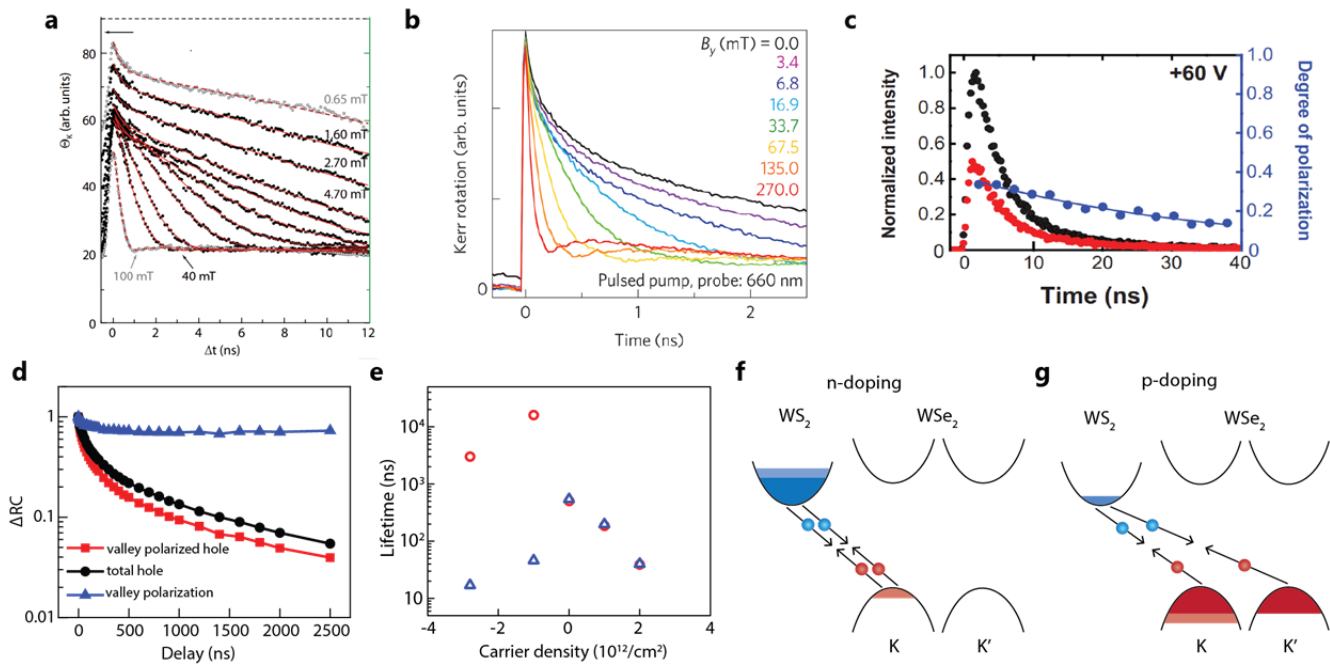446
447
448
449

Fig. 4 **Dynamics of spin-valley information carriers in TMDC materials**. (a-b) Spin-valley dynamics of trions (a)[72] and resident electrons (b)[81] in monolayer TMDC materials under different external magnetic fields as probed by time-resolved Kerr rotation measurements. A spin-valley lifetime of few to tens of nanoseconds is observed at low fields. (c) Time-resolved photoluminescence in a nearly aligned $WSe_2/MoSe_2$ heterobilayer for the same (black) and opposite (red) circularly polarized excitation, revealing a valley lifetime of few nanoseconds[84]. (d) Decay dynamics of the valley-polarized hole population, the total hole population, and the valley polarization in a large-twist-angle WSe_2/MoS_2 heterostructure at charge neutrality[94]. (e) Summary of the hole population (blue) and spin-valley (red) lifetimes as a function of carrier concentration in a large-twist-angle WSe_2/WS_2 heterostructure[95]. (f-g) Schematic illustration of the interlayer electron-hole recombination process in electron-doped (f) and hole-doped (g) heterostructures.

Potential mechanism behind intervalley scattering

As discussed in the previous sections, the spin-valley lifetime can be limited either by the population lifetime or by the intervalley scattering process. The first limitation can be removed for valley-polarized holes in hole-doped heterostructures, making them promising candidates for spin-valley information carriers. Furthermore, directly probing hole dynamics provides relatively clean information about the decay mechanism owing to the simplicity of the valence band maximum. This configuration thus provides a valuable platform for understanding intervalley scattering processes in TMDC materials.

Figure 5a shows the decay dynamics of valley polarization at different temperature for holes in WSe_2/MoS_2 heterostructures, with the valley depolarization lifetime summarized in Fig. 5b (Ref. [94]).

479   The depolarization lifetime changes from 10 ns at 77 K to above 40 µs at 10 K, which roughly follows

480   a thermally activated rate: $\tau \sim exp\left(\frac{\Delta}{k_B T}\right)$, with k_B denoting the Boltzmann constant and $\Delta \sim$ 20 meV.

481

482
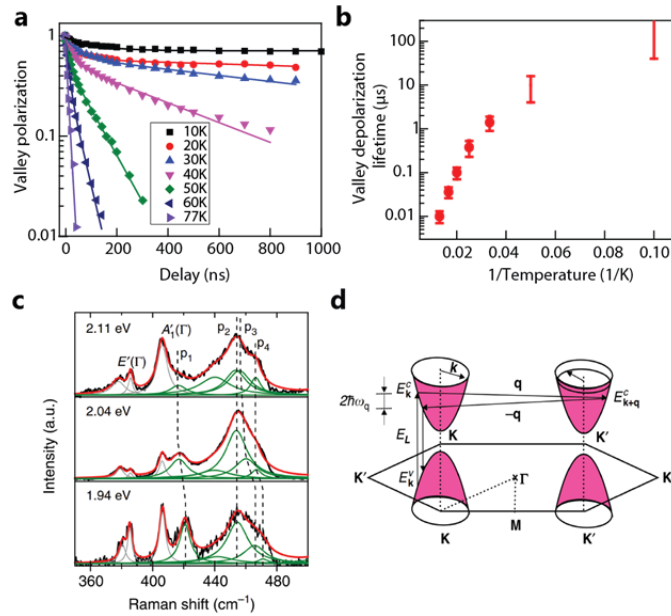
483
484   Fig. 5 **Potential origin of intervalley scattering in** WSe$_2$/MoS$_2$
485   heterostructures. (a) Temperature-dependent decay dynamics of valley
486   polarization. (b) Temperature dependence of the intervalley scattering
487   time. The process can be described as thermally activated[94]. (c)
488   Resonant Raman spectra of single-layer MoS$_2$ show particularly strong
489   second-order Raman signals (peaks p1 to p4) for excitation around 2.0
490   eV through a doubly resonant Raman (DRR) process involving K point
491   phonons, as illustrated in (d)[96].

492

493   The inter-valley scattering of holes in WSe$_2$ requires a large momentum change and a simultaneous

494   spin flip. However, due to the strong spin-orbit coupling in WSe$_2$, the picture of electrons and holes

495   with perfectly defined up and down spin states in the K and K' valleys, respectively, is not strictly valid

496   for states away from the K and K' points. Therefore, inter-valley scattering of carriers near, but not

497   exactly at K and K' points is allowed. This process, often designated as the Elliott-Yafet mechanism,

498   has a characteristic temperature dependence of

$$\tau_{EY}^{-1} \sim T^2\, \tau_p^{-1},$$

499   where τ_p is the momentum scattering lifetime for a spin-conserving process. The T^2 -dependence

500   originates from the fact that at higher temperature, thermally excited carriers are further away from

501   band minima (K or K') and will therefore scatter more efficiently. However, the predicted T^2

502   dependence does not describe the strong observed variation with temperature, which presumably

503   reflects from the temperature dependence of τ_p^{-1}. Indeed, a thermally activated temperature

504   dependence is expected for phonon-assisted intervalley scattering at low temperatures, and the

505   experimental activation energy of ~20 meV agrees with WSe$_2$ phonon energy (at the K-point) required

506   for intervalley scattering[96]. Phonon-assisted intervalley scattering, accompanied by spin flip through

507   the Elliott-Yafet mechanism, can thus account for the observed spin-valley depolarization of holes.

508

509 The important role of K-point phonons in intervalley scattering is also supported by a recent resonant
510 Raman study[96], which reveals second-order Raman signals (peaks p1 to p4 in Fig. 5c) assigned to K-
511 point phonons through a doubly resonant Raman (DRR) scattering process. This observation
512 suggests a strong interaction between charge carriers and K-point phonons, which dramatically
513 enhances their second-order Raman signals through the DRR process illustrated in Fig. 5d.
514

Spin-valley transport in TMDC heterostructures

516 The efficient generation of pure spin-valley imbalance in hole-doped WSe_2/WS_2 heterostructures
517 provides a convenient way to create pure spin-valley current (Fig. 6a), which lies in the heart of spin-
518 valley-tronic devices. Jin *et al.* performed space-and-time-resolved pump-probe spectroscopy to track
519 the evolution of the spin-valley imbalance and to image the flow of pure spin-valley diffusion currents
520 (Fig. 6b). Figure 6c shows experimental results for a hole-doped WS_2/WSe_2 heterostructure at an
521 initial electrostatic hole doping of $p_0 = 1 \times 10^{12}$ /cm^2. At zero time delay, the spin-valley imbalance
522 matches the pump beam spatial profile (half-width of ~1.5 μm); the signal is negligible for a pump-
523 probe separations greater than 3 μm, as expected based on the convolution with probe spatial profile.
524 At finite delay time, the spin-valley imbalance diffuses out of the excitation region, generating a pure
525 spin-valley current. This leads to a strong decrease and increase of signal, respectively, in regions
526 near and far away from the pump beam. The spin-valley current propagates to distances over 8 μm
527 within 800 ns. Such direct imaging of the experimental spin-valley current flow (Fib. 6c) allows us to
528 determine important physical parameters by comparison with a diffusion-decay model (Fig. 6d). We
529 infer a diffusion constant of $D = 0.2$ cm$^2/s$, a spin-valley lifetime of $\tau = 20$ μs, and deduce a spin-valley
530 diffusion length of $l = \sqrt{D\tau} = 20$ μm.
531
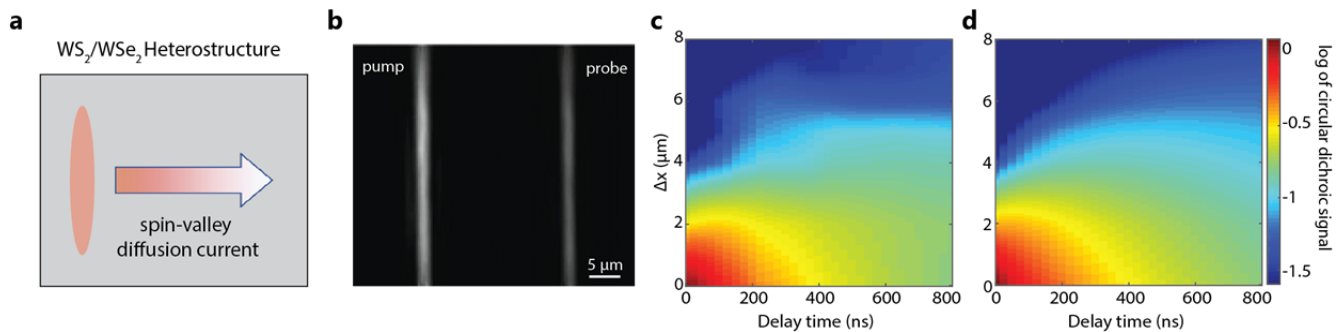
534 Fig. 6 **Spin-valley transport in a vdW heterostructure**[95]. (a) Optical
535 excitation of pure spin-valley imbalance at the left edge of a device will
536 create a pure spin-valley diffusion current flowing to the right without any
537 associated charge current. (b) Experimental configuration for direct
538 imaging of the spin-valley current flow with space-and-time resolved
539 pump-probe spectroscopy using pump and probe beams focused to lines
540 on the sample at defined spatial separation. (c-d) Experimentally
541 measured spatio-temporal evolution of the pure valley imbalance in the
542 heterostructure (c) and a simulation of the results using a diffusion-decay
543 model (d) for an initial hole doping of 10^{12}/cm^2.
544

545 The efficient generation of spin-valley current with remarkably large current densities reflects the
546 nearly ideal conversion of photogenerated excitons into a spin-valley imbalance. Still higher spin-

547   valley currents may be achievable in TMDC heterostructures by increasing the initial hole doping
548   level to enable stronger optical pumping, as well as by improving the device quality to enhance the
549   diffusivity. The long spin-valley lifetimes and diffusion lengths of valley-polarized holes in TDMC
550   heterostructures hold promise for the generation, transport, and detection of spin-valley information
551   and open exciting opportunities for the realization of future spintronic and valleytronic devices.
552

553   **Concluding remarks**
554   Despite the rapid progress in the study of excited-states in van der Waals heterostructures
555   summarized above, many outstanding questions remain in understanding charge transfer processes
556   and the spin and valley relaxation dynamics.
557

558   A complete picture of the underlying mechanism for the CT process in TMDC heterostructures
559   remains elusive. First, the mechanisms developed to date do not account for the Coulombic
560   interactions between electrons and holes, despite the existence of strongly bound excitons both in the
561   TMDC monolayers[8,97,98] and in the heterostructures[40]. Though one can argue that the excitonic states
562   are superpositions of the quasiparticle band states and, hence, are affected similarly, a quantitative
563   picture in which excitonic correlations are taken into account remains a theoretical challenge. In this
564   context, it would also be interesting to learn whether the dielectric environment of the heterostructure,
565   which affects the excitonic interactions, also significantly influences the rate and efficiency of CT
566   processes. In addition, the fact that changes in the dielectric screening of Coulombic interactions in
567   TMDCs modify the quasiparticle band structure may provide a route to test the role of the Q and Γ
568   valleys in CT processes. Second, the time-domain probes of CT to date have been limited in their by
569   the instrumental response function and have not generally yielded precise CT times. In addition,
570   optical measurements, with their limited spatial resolution, average over moiré patterns formed
571   between the two layers. This may lead to a washing out of predicted trends for CT times. Overcoming
572   these limitations by improved temporal resolution and/or spatial resolution (such as through near-field
573   techniques) would provide important experimental information to inform and test further theoretical
574   models.
575

576   Similarly many outstanding questions exist regarding spin and valley dynamics in TMDC
577   heterostructures. Much more work is required to understand fully the intrinsic spin and valley
578   dynamics in TMDC heterostructures and the dependence of the dynamics on the constituent TMDC
579   materials, their relative crystallographic alignment, and their stacking order in multilayers. It remains,
580   for example, unclear what factors define the ultimate limit for the spin-valley lifetime in TMDC
581   heterostructures; also unknown is the role played by defects, edges, and grain boundaries, as well as
582   possible effects from large-period moiré superlattices formed in TMDC heterostructures with small
583   twist angles.
584

585

References

588 1 Hunt, B. *et al.* Massive Dirac Fermions and Hofstadter Butterfly in a van der Waals
589 Heterostructure. *Science* **340**, 1427-1430, (2013).
590 2 Ponomarenko, L. A. *et al.* Cloning of Dirac fermions in graphene superlattices. *Nature* **497**,
591 594-597, (2013).
592 3 Dean, C. R. *et al.* Hofstadter's butterfly and the fractal quantum Hall effect in moire
593 superlattices. *Nature* **497**, 598-602, (2013).
594 4 Spanton, E. M. *et al.* Observation of fractional Chern insulators in a van der Waals
595 heterostructure. *Science* **360**, 62-66, (2018).
596 5 Cao, Y. *et al.* Unconventional superconductivity in magic-angle graphene superlattices. *Nature*
597 **556**, 43-+, (2018).
598 6 Cao, Y. *et al.* Correlated insulator behaviour at half-filling in magic-angle graphene
599 superlattices. *Nature* **556**, 80-+, (2018).
600 7 Chen, G. *et al.* Gate-Tunable Mott Insulator in Trilayer Graphene-Boron Nitride Moiré
601 Superlattice. *Arxiv*, 1803.01985, (2018).
602 8 Chernikov, A. *et al.* Exciton Binding Energy and Nonhydrogenic Rydberg Series in Monolayer
603 WS2. *Phys Rev Lett* **113**, (2014).
604 9 Ye, Z. L. *et al.* Probing excitonic dark states in single-layer tungsten disulphide. *Nature* **513**,
605 214-218, (2014).
606 10 Xiao, D., Liu, G. B., Feng, W. X., Xu, X. D. & Yao, W. Coupled Spin and Valley Physics in
607 Monolayers of MoS2 and Other Group-VI Dichalcogenides. *Phys Rev Lett* **108**, (2012).
608 11 Xu, X. D., Yao, W., Xiao, D. & Heinz, T. F. Spin and pseudospins in layered transition metal
609 dichalcogenides. *Nat Phys* **10**, 343-350, (2014).
610 12 Komsa, H. P. & Krasheninnikov, A. V. Electronic structures and optical properties of realistic
611 transition metal dichalcogenide heterostructures from first principles. *Phys Rev B* **88**, (2013).
612 13 Gong, C. *et al.* Band alignment of two-dimensional transition metal dichalcogenides:
613 Application in tunnel field effect transistors. *Appl Phys Lett* **103**, (2013).
614 14 Terrones, H., Lopez-Urias, F. & Terrones, M. Novel hetero-layered materials with tunable
615 direct band gaps by sandwiching different metal disulfides and diselenides. *Sci Rep-Uk* **3**,
616 (2013).
617 15 Stormer, H. L., Dingle, R., Gossard, A. C., Wiegmann, W. & Sturge, M. D. 2-Dimensional
618 Electron-Gas at a Semiconductor-Semiconductor Interface. *Solid State Commun* **29**, 705-709,
619 (1979).
620 16 Bellus, M. Z. *et al.* Type-I van der Waals heterostructure formed by MoS2 and ReS2
621 monolayers. *Nanoscale Horiz* **2**, 31-36, (2017).
622 17 Chiu, M. H. *et al.* Determination of band alignment in the single-layer MoS2/WSe2
623 heterojunction. *Nat Commun* **6**, (2015).
624 18 Ozcelik, V. O., Azadani, J. G., Yang, C., Koester, S. J. & Low, T. Band alignment of two-
625 dimensional semiconductors for designing heterostructures with momentum space matching.
626 *Phys Rev B* **94**, (2016).
627 19 Hong, X. P. *et al.* Ultrafast charge transfer in atomically thin MoS2/WS2 heterostructures. *Nat*
628 *Nanotechnol* **9**, 682-686, (2014).
629 20 Wang, K. *et al.* Interlayer Coupling in Twisted WSe2/WS2 Bilayer Heterostructures Revealed
630 by Optical Spectroscopy. *Acs Nano* **10**, 6612-6622, (2016).
631 21 Kozawa, D. *et al.* Evidence for Fast Interlayer Energy Transfer in MoSe2/WS2
632 Heterostructures. *Nano Lett* **16**, 4087-4093, (2016).
633 22 Zhang, C. X. *et al.* Systematic study of electronic structure and band alignment of monolayer
634 transition metal dichalcogenides in Van der Waals heterostructures. *2d Mater* **4**, (2017).

635 23 Debbichi, L., Eriksson, O. & Lebegue, S. Electronic structure of two-dimensional transition
636   metal dichalcogenide bilayers from ab initio theory. *Phys Rev B* **89**, (2014).
637 24 Zhang, J. F., Xie, W. Y., Zhao, J. J. & Zhang, S. B. Band alignment of two-dimensional lateral
638   heterostructures. *2d Mater* **4**, (2017).
639 25 Qiu, D. Y., da Jornada, F. H. & Louie, S. G. Screening and many-body effects in two-
640   dimensional crystals: Monolayer MoS2. *Phys Rev B* **93**, (2016).
641 26 Wilson, N. R. *et al.* Determination of band offsets, hybridization, and exciton binding in 2D
642   semiconductor heterostructures. *Sci Adv* **3**, (2017).
643 27 Hill, H. M., Rigosi, A. F., Rim, K. T., Flynn, G. W. & Heinz, T. F. Band Alignment in MoS2/WS2
644   Transition Metal Dichalcogenide Heterostructures Probed by Scanning Tunneling Microscopy
645   and Spectroscopy. *Nano Lett* **16**, 4831-4837, (2016).
646 28 Ceballos, F., Bellus, M. Z., Chiu, H. Y. & Zhao, H. Ultrafast Charge Separation and Indirect
647   Exciton Formation in a MoS2-MoSe2 van der Waals Heterostructure. *Acs Nano* **8**, 12717-
648   12724, (2014).
649 29 Heo, H. *et al.* Interlayer orientation-dependent light absorption and emission in monolayer
650   semiconductor stacks. *Nat Commun* **6**, (2015).
651 30 Zhu, H. M. *et al.* Interfacial Charge Transfer Circumventing Momentum Mismatch at Two-
652   Dimensional van der Waals Heterojunctions. *Nano Lett* **17**, 3591-3598, (2017).
653 31 Ji, Z. H. *et al.* Robust Stacking-Independent Ultrafast Charge Transfer in MoS2/WS2 Bilayers.
654   *Acs Nano* **11**, 12020-12026, (2017).
655 32 Chen, H. L. *et al.* Ultrafast formation of interlayer hot excitons in atomically thin MoS2/WS2
656   heterostructures. *Nat Commun* **7**, (2016).
657 33 Ceballos, F., Ju, M. G., Lane, S. D., Zeng, X. C. & Zhao, H. Highly Efficient and Anomalous
658   Charge Transfer in van der Waals Trilayer Semiconductors. *Nano Lett* **17**, 1623-1628, (2017).
659 34 Lee, C.-H. *et al.* Atomically thin p-n junctions with van der Waals heterointerfaces. *Nat
660   Nanotechnol* **9**, 676, (2014).
661 35 Rigos, A. F., Hill, H. M., Li, Y. L., Chernikov, A. & Heinz, T. F. Probing Interlayer Interactions in
662   Transition Metal Dichalcogenide Heterostructures by Optical Spectroscopy: MoS2/WS2 and
663   MoSe2/WSe2. *Nano Lett* **15**, 5033-5038, (2015).
664 36 Pan, S. D., Ceballos, F., Bellus, M. Z., Zereshki, P. & Zhao, H. Ultrafast charge transfer
665   between MoTe2 and MoS2 monolayers. *2d Mater* **4**, (2017).
666 37 Xu, W. G. *et al.* Correlated fluorescence blinking in two-dimensional semiconductor
667   heterostructures. *Nature* **541**, 62-+, (2017).
668 38 Ceballos, F., Bellus, M. Z., Chiu, H. Y. & Zhao, H. Probing charge transfer excitons in a
669   MoSe2-WS2 van der Waals heterostructure. *Nanoscale* **7**, 17523-17528, (2015).
670 39 Li, Y. Y. *et al.* Ultrafast Interlayer Electron Transfer in Incommensurate Transition Metal
671   Dichalcogenide Homobilayers. *Nano Lett* **17**, 6661-6666, (2017).
672 40 Rivera, P. *et al.* Observation of long-lived interlayer excitons in monolayer MoSe2-WSe2
673   heterostructures. *Nat Commun* **6**, (2015).
674 41 Robert, C. *et al.* Exciton radiative lifetime in transition metal dichalcogenide monolayers. *Phys
675   Rev B* **93**, (2016).
676 42 Xu, W. S. *et al.* Determining the Optimized Interlayer Separation Distance in Vertical Stacked
677   2D WS2:hBN:MoS2 Heterostructures for Exciton Energy Transfer. *Small* **14**, (2018).
678 43 Mak, K. F., Lee, C., Hone, J., Shan, J. & Heinz, T. F. Atomically Thin MoS2: A New Direct-Gap
679   Semiconductor. *Phys Rev Lett* **105**, (2010).
680 44 Splendiani, A. *et al.* Emerging Photoluminescence in Monolayer MoS2. *Nano Lett* **10**, 1271-
681   1275, (2010).
682 45 Zhu, X. Y. *et al.* Charge Transfer Excitons at van der Waals Interfaces. *J Am Chem Soc* **137**,
683   8313-8320, (2015).
684 46 Wang, H. *et al.* The role of collective motion in the ultrafast charge transfer in van der Waals
685   heterostructures. *Nat Commun* **7**, (2016).
686 47 Zhang, J. *et al.* Interlayer-State-Coupling Dependent Ultrafast Charge Transfer in MoS2/WS2
687   Bilayers. *Adv Sci* **4**, (2017).

688 48 Long, R. & Prezhdo, O. V. Quantum Coherence Facilitates Efficient Charge Separation at a
689   MoS2/MoSe2 van der Waals Junction. *Nano Lett* **16**, 1996-2003, (2016).
690 49 Li, L. Q., Long, R. & Prezhdo, O. V. Charge Separation and Recombination in Two-
691   Dimensional MoS2/WS2: Time-Domain ab Initio Modeling. *Chem Mater* **29**, 2466-2473, (2017).
692 50 Kang, J., Li, J. B., Li, S. S., Xia, J. B. & Wang, L. W. Electronic Structural Moire Pattern Effects
693   on MoS2/MoSe2 2D Heterostructures. *Nano Lett* **13**, 5485-5490, (2013).
694 51 Tong, Q. J. *et al.* Topological mosaics in moire superlattices of van der Waals heterobilayers.
695   *Nat Phys* **13**, 356-362, (2017).
696 52 Wang, Y., Wang, Z., Yao, W., Liu, G. B. & Yu, H. Y. Interlayer coupling in commensurate and
697   incommensurate bilayer structures of transition-metal dichalcogenides. *Phys Rev B* **95**, (2017).
698 53 Zheng, Q. J. *et al.* Phonon-Assisted Ultrafast Charge Transfer at van der Waals
699   Heterostructure Interface. *Nano Lett* **17**, 6435-6442, (2017).
700 54 Jin, C. H. *et al.* On Optical Dipole Moment and Radiative Recombination Lifetime of Excitons
701   in WSe2. *Adv Funct Mater* **27**, (2017).
702 55 Zhang, X. X., You, Y. M., Zhao, S. Y. F. & Heinz, T. F. Experimental Evidence for Dark
703   Excitons in Monolayer WSe2. *Phys Rev Lett* **115**, (2015).
704 56 Korn, T., Heydrich, S., Hirmer, M., Schmutzler, J. & Schuller, C. Low-temperature photocarrier
705   dynamics in monolayer MoS2. *Appl Phys Lett* **99**, (2011).
706 57 Amani, M. *et al.* Near-unity photoluminescence quantum yield in MoS2. *Science* **350**, 1065-
707   1068, (2015).
708 58 Moody, G. *et al.* Intrinsic homogeneous linewidth and broadening mechanisms of excitons in
709   monolayer transition metal dichalcogenides. *Nat Commun* **6**, (2015).
710 59 Lagarde, D. *et al.* Carrier and Polarization Dynamics in Monolayer MoS2. *Phys Rev Lett* **112**,
711   (2014).
712 60 Wang, Q. S. *et al.* Valley Carrier Dynamics in Mono layer Molybdenum Disulfide from Helicity-
713   Resolved Ultrafast Pump-Probe Spectroscopy. *Acs Nano* **7**, 11087-11093, (2013).
714 61 Hao, K. *et al.* Direct measurement of exciton valley coherence in monolayer WSe2. *Nat Phys*
715   **12**, 677-+, (2016).
716 62 Mai, C. *et al.* Many-Body Effects in Valleytronics: Direct Measurement of Valley Lifetimes in
717   Single-Layer MoS2. *Nano Lett* **14**, 202-206, (2014).
718 63 Zhu, C. R. *et al.* Exciton valley dynamics probed by Kerr rotation in WSe2 monolayers. *Phys
719   Rev B* **90**, (2014).
720 64 Mak, K. F., He, K. L., Shan, J. & Heinz, T. F. Control of valley polarization in monolayer MoS2
721   by optical helicity. *Nat Nanotechnol* **7**, 494-498, (2012).
722 65 Zeng, H. L., Dai, J. F., Yao, W., Xiao, D. & Cui, X. D. Valley polarization in MoS2 monolayers
723   by optical pumping. *Nat Nanotechnol* **7**, 490-493, (2012).
724 66 Cao, T. *et al.* Valley-selective circular dichroism of monolayer molybdenum disulphide. *Nat
725   Commun* **3**, (2012).
726 67 Glazov, M. M. *et al.* Exciton fine structure and spin decoherence in monolayers of transition
727   metal dichalcogenides. *Phys Rev B* **89**, (2014).
728 68 Yu, T. & Wu, M. W. Valley depolarization due to intervalley and intravalley electron-hole
729   exchange interactions in monolayer MoS2. *Phys Rev B* **89**, (2014).
730 69 Yu, H. Y., Liu, G. B., Gong, P., Xu, X. D. & Yao, W. Dirac cones and Dirac saddle points of
731   bright excitons in monolayer transition metal dichalcogenides. *Nat Commun* **5**, (2014).
732 70 Maialle, M. Z., Silva, E. A. D. E. & Sham, L. J. Exciton Spin Dynamics in Quantum-Wells. *Phys
733   Rev B* **47**, 15776-15788, (1993).
734 71 Hao, K. *et al.* Trion valley coherence in monolayer semiconductors. *2d Mater* **4**, (2017).
735 72 Volmer, F. *et al.* Intervalley dark trion states with spin lifetimes of 150 ns in WSe2. *Phys Rev B*
736   **95**, (2017).
737 73 Plechinger, G. *et al.* Trion fine structure and coupled spin-valley dynamics in monolayer
738   tungsten disulfide. *Nat Commun* **7**, (2016).
739 74 Zhang, X. X. *et al.* Magnetic brightening and control of dark excitons in monolayer WSe2. *Nat
740   Nanotechnol* **12**, 883-+, (2017).

741 75 Jiang, C. Y. *et al.* Microsecond dark-exciton valley polarization memory in two-dimensional
742   heterostructures. *Nat Commun* **9**, (2018).
743 76 You, Y. M. *et al.* Observation of biexcitons in monolayer WSe2. *Nat Phys* **11**, 477-U138,
744   (2015).
745 77 Chen, S., Goldstein, T., Taniguchi, T., Watanabe, K. & Yan, J. Coulomb-bound four- and five-
746   particle valleytronic states in an atomically-thin semiconductor. *Arxiv*, 1802.10247, (2018).
747 78 Dey, P. *et al.* Gate-Controlled Spin-Valley Locking of Resident Carriers in WSe2 Monolayers.
748   *Phys Rev Lett* **119**, (2017).
749 79 Song, X. L., Xie, S. E., Kang, K., Park, J. & Sih, V. Long-Lived Hole Spin/Valley Polarization
750   Probed by Kerr Rotation in Monolayer WSe2. *Nano Lett* **16**, 5010-5014, (2016).
751 80 Hsu, W. T. *et al.* Optically initialized robust valley-polarized holes in monolayer WSe2. *Nat
752   Commun* **6**, (2015).
753 81 Yang, L. Y. *et al.* Long-lived nanosecond spin relaxation and spin coherence of electrons in
754   monolayer MoS2 and WS2. *Nat Phys* **11**, 830-U187, (2015).
755 82 Fang, H. *et al.* Strong interlayer coupling in van der Waals heterostructures built from single-
756   layer chalcogenides. *P Natl Acad Sci USA* **111**, 6198-6202, (2014).
757 83 Nagler, P. *et al.* Interlayer exciton dynamics in a dichalcogenide monolayer heterostructure. *2d
758   Mater* **4**, (2017).
759 84 Rivera, P. *et al.* Valley-polarized exciton dynamics in a 2D semiconductor heterostructure.
760   *Science* **351**, 688-691, (2016).
761 85 Hsu, W. T. *et al.* Negative circular polarization emissions from WSe2/MoSe2 commensurate
762   heterobilayers. *Nat Commun* **9**, (2018).
763 86 Hanbicki, A. T. *et al.* Double Indirect Interlayer Exciton in a MoSe2/WSe2 van der Waals
764   Heterostructure. *Arxiv*, 1802.05310, (2018).
765 87 Ciarrocchi, A. *et al.* Control of interlayer excitons in two-dimensional van der Waals
766   heterostructures. *Arxiv*, 1803.06405, (2018).
767 88 Yu, H. Y., Wang, Y., Tong, Q. J., Xu, X. D. & Yao, W. Anomalous Light Cones and Valley
768   Optical Selection Rules of Interlayer Excitons in Twisted Heterobilayers. *Phys Rev Lett* **115**,
769   (2015).
770 89 Yu, H. Y., Liu, B. L. & Yao, W. Brightened spin-triplet interlayer excitons and optical selection
771   rules in van der Waals heterobilayers. 1803.01292, (2018).
772 90 Miller, B. *et al.* Long-Lived Direct and Indirect Interlayer Excitons in van der Waals
773   Heterostructures. *Nano Lett* **17**, 5229-5237, (2017).
774 91 Kunstmann, J. *et al.* Momentum-space indirect interlayer excitons in transition-metal
775   dichalcogenide van der Waals heterostructures. *Nat Phys*, (2018).
776 92 Wu, F. C., Lovorn, T. & MacDonald, A. H. Theory of optical absorption by interlayer excitons in
777   transition metal dichalcogenide heterobilayers. *Phys Rev B* **97**, (2018).
778 93 Yu, H. Y., Liu, G. B., Tang, J. J., Xu, X. D. & Yao, W. Moire excitons: From programmable
779   quantum emitter arrays to spin-orbit-coupled artificial lattices. *Sci Adv* **3**, (2017).
780 i94 Kim, J. *et al.* Observation of ultralong valley lifetime in WSe2/MoS2 heterostructures. *Sci Adv*
781   **3**, (2017).
782 95 Jin, C. H. *et al.* Imaging of Pure Spin-Valley Diffusion Current in WS2/WSe2 Heterostructures.
783   *Science*, in press, (2018).
784 96 Carvalho, B. R. *et al.* Intervalley scattering by acoustic phonons in two-dimensional MoS2
785   revealed by double-resonance Raman spectroscopy. *Nat Commun* **8**, (2017).
786 97 Hill, H. M. *et al.* Observation of Excitonic Rydberg States in Monolayer MoS2 and WS2 by
787   Photoluminescence Excitation Spectroscopy. *Nano Lett* **15**, 2992-2997, (2015).
788 98 He, K. L. *et al.* Tightly Bound Excitons in Monolayer WSe2. *Phys Rev Lett* **113**, (2014).
789

790